iJRASET
International Journal For Research in Applied Science and Engineering Technology

# INTERNATIONAL JOURNAL FOR RESEARCH

IN APPLIED SCIENCE & ENGINEERING TECHNOLOGY

**Volume:** 9 **Issue:** IX **Month of publication:** September 2021

**DOI:** https://doi.org/10.22214/ijraset.2021.38257

www.ijraset.com

Call: 08813907089 | E-mail ID: ijraset@gmail.com

International Journal for Research in Applied Science & Engineering Technology (IJRASET)
*ISSN: 2321-9653; IC Value: 45.98; SJ Impact Factor: 7.429*
*Volume 9 Issue IX Sep 2021- Available at www.ijraset.com*

# Design of Off-Grid Solar Photovoltaic and Energy Storage System for Slow Pyrolysis Reactor

Karan Bhatia[1], Khush Furia[2]
[1, 2]*Student, Department of Mechanical Engineering, K.J. Somaiya College of Engineering, Mumbai, India.*

***Abstract*: *The need for sustainable methods of producing energy is growing now more than ever due to the increasing environmental concerns and the current climate crisis. By combining the existing pyrolysis setup available to us, with solar energy, we can help in reducing the carbon footprint of the setup. India is one of the largest agrarian economies and as a result produces vast amounts of biomass waste, which is disposed of by burning. This produces a lot of smoke which contributes to a thick hazy smog in northern India and has a serious impact on the health of its population. Research in the thermo-chemical conversion of biomass waste and polymer wastes has also gained momentum in recent years. Various methods have been developed to reduce agricultural biomass and plastic wastes, but the Pyrolysis process proves its effectiveness in reducing wastes as well as converting them into useful fuels. Pyrolysis is a relatively simple, inexpensive, and robust thermo-chemical technology for transforming biomass into bio-oil, biochar, and syngas. In this report, we focused on how to make the pyrolysis process more efficient, eco-friendly, and cost-effective by combining it with a solar photovoltaic system. A Photovoltaic (PV) system also helps in decreasing the grid dependence and increasing the reliability of the pyrolysis setup. It is used in conjunction with lithium-ion batteries to provide the necessary power required to carry out the pyrolytic conversion. Thus, with this solution, we can effectively produce energy while getting rid of bulky organic and plastic waste.***

***Keywords: Pyrolysis, Sustainable energy, Solar Energy, Renewable Energy, Solar Photovoltaic System, Lithium-ion batteries.***

**Nomenclature**

| | |
|---|---|
| *OEM* | Original Equipment Manufacturer |
| *BMS* | Battery Management System |
| *PCU* | Power Conditioning Unit |
| *PV* | Photovoltaic |
| *MCB* | Miniature Circuit Breaker |
| *RES* | Renewable Energy Sources |
| *MPPT* | Maximum Power Point Tracking |
| *ESH* | Effective Sun Hours |
| *TDS* | Technical Data Sheet |
| *DOD* | Depth Of Discharge |

## I. INTRODUCTION

Energy has become a both, valuable and omnipresent commodity in present times. It affects every aspect of life, right from an individual level to that of whole countries. We must therefore learn to use energy responsibly and efficiently such that we can meet both our current and future demands of energy. Unlike renewable energy sources, fossil fuels are of depleting or non-renewable nature. Moreover, burning fossil fuels is causing rapid climate change which will lead to the loss of both lives and livelihood. On the other hand, Biomass fuels and other renewable energy sources can be made net carbon neutral, fulfilling the nation's energy needs while not contributing to the climate change crisis that the world faces today.

### *A. Motivation*

India is a country, where agriculture is not only one of the major contributors to the national GDP, but also source of employment to a large part of our country's population. This makes is prudent, that the technology and solutions which help this sector and the environment should be studied as well as implemented. One of the major problems faced by farmers is the disposal of the waste and the byproducts of their harvest.

Not only that, they also need to clear the field to prepare it for the next cycle of harvesting period for sowing new crops. The easiest and the most cost-efficient way for the farmers, is to incinerate the field and burn the waste products. This however has a serious environmental impact and that on public health. Crop residue burning is a serious environmental issue in India. It releases harmful toxic gases and particulate matter (PM) in air which later results in breathing related diseases.

India produces around 500 million tons of agricultural waste a year. The burning of this much crop residues creates various environmental problems. The main adverse effects of this burning include the emission of greenhouse gases (GHGs) that contribute to global warming, increased levels of particulate matter (PM) and smog that causes health hazards, loss of biodiversity of farmlands, and the degradation of soil fertility. The PM emitted out by the burning of crop residues in Delhi is 17 times that from all other sources such as vehicle emissions, garbage burning, and industries combine. [1]

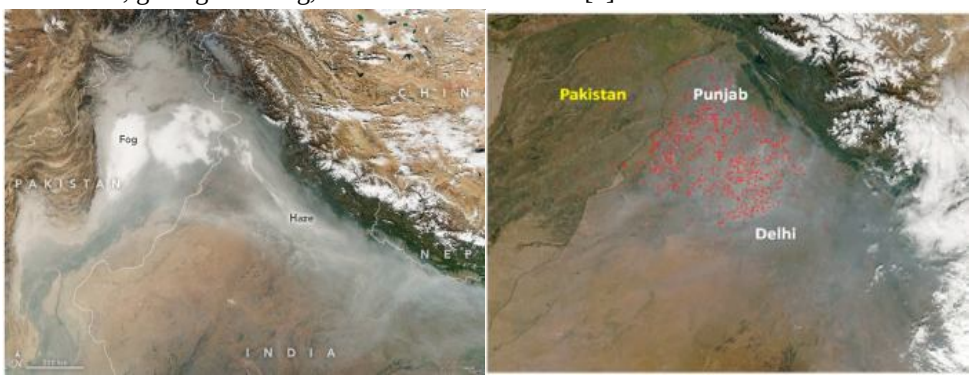


Fig. 1: Pollution due to Crop Burning (Courtesy: NASA)

Moreover, India is a country with an abundance of solar insolation almost all year long. It is an energy resource that has gained recognition only in recent times and even today, is quite under-utilized.

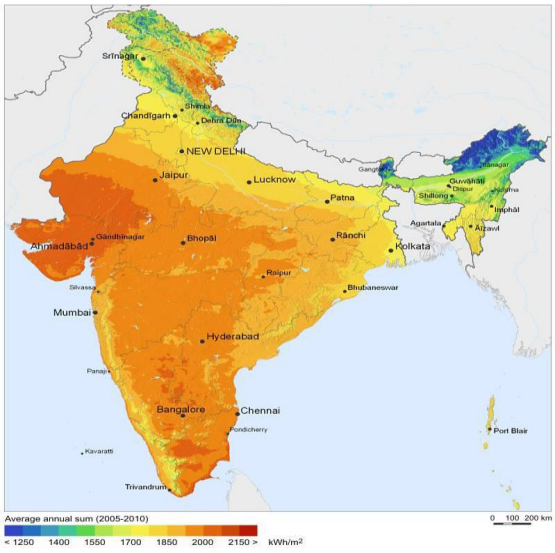


Fig. 2: Solar irradiation in India. [2]

From the figure above, it can be observed that India receives anywhere between 4-6 kWh of energy a day depending on the location. This project was inspired by both, the waste disposal and energy crises that the world faces today.

*B. Pyrolysis*

Pyrolysis is a process wherein biomass undergoes thermo chemical decomposition in absence of oxygen or with a finite supply of air that does not permit gasification to an appreciable extent. During pyrolysis higher hydrocarbon chains break down into relatively smaller and simpler molecules of solid, liquid and gas. Pyrolysis of biomass is carried out at low moderate temperatures in the range 400-600$^0$C. Pyrolysis has been used since history to transform wood into charcoal. Today pyrolysis is being developed as a waste to energy technology to convert biomass and plastic waste into liquid fuels. [3].

Pyrolysis products always produce solid (charcoal, biochar), liquid and non-condensable gases ($H_2$, $CH_4$, CnHm, CO, $CO_2$ and $N_2$). Because the liquid phase is extracted from pyrolysis gas only during its cooling down, in some applications, these two streams will be used together when providing hot syngas on to the burner or oxidation chamber. During the pyrolysis, a particle of waste is heated from the ambient to defined temperature. The waste remains inside the pyrolysis unit and is carried by screw conveyor at fixed speed, till the completion of the process. The chosen temperature of pyrolysis defines the composition and yields of products. Products of pyrolysis depend on pyrolyzer, physical and chemical characteristics of biomass and operating parameters such as Product Residence Time in Reactor, Pyrolysis Temperature and Particle Size [3].

### *C. Background*

The existing pyrolysis reactor is a grid-powered electric muffle furnace type reactor with a maximum power draw of 4.5kW. The precise pyrolytic temperature and ramp is controlled by a Programmable Logic Controller (PLC) which reads inputs from a thermistor.

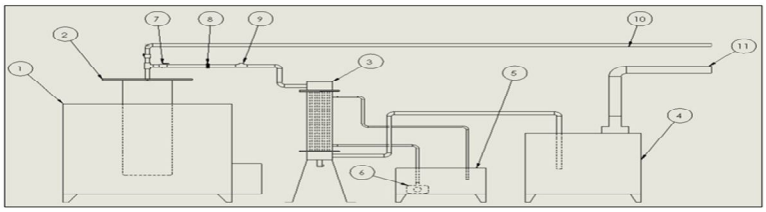

| NO. | Component | NO. | Component | NO. | Component | NO. | Component |
|---|---|---|---|---|---|---|---|
| 1 | Muffle Furnace | 4 | Water Scrubber | 7 | Ball Valve | 10 | Emergency Exhaust |
| 2 | Pyrolysis reactor | 5 | Pump Water tank | 8 | Union Joint | 11 | Uncondensed gas |
| 3 | Gas Condenser (HE) | 6 | Submersible Pump | 9 | Non Return Valve | | |

Fig. 3**:** Schematic of Reactor setup

As can be seen from fig.3, the setup also incorporates Non-Return Valves to prevent water from being pulled into the hot reactor by the vacuum created in the slowly cooling reactor chamber. The setup also has such supporting components as a heat exchanger for bio-oil collection and a water scrubber to remove particulate matter and condensable gases. The reactor is capable of handling slow and medium speed pyrolysis and materials ranging from biomass to plastics and a mixture of both i.e., Co-Pyrolysis.

## II. SOLAR PHOTOVOLTAIC SYSTEM DESIGN

Since this project is meant to be eventually implemented in rural areas of the country, an off grid or hybrid system architecture was chosen with the aim of supplying enough energy to run the reactor in all conditions. Solar PV was chosen since they offer many advantages over thermal collectors: Photovoltaics are more flexible in operation, with ease of maintenance of the system, convenient storage of energy, the capability to run additional equipment off the electricity generated and the ability to run the reactor at night or pulling power from the grid in case of failure, to name a few [4]. The following sections will explore the design in detail.

### *A. Load Calculations*

The table below summarizes the calculations for determining the loading conditions and energy requirements for the setup.

TABLE I
Summary of Energy Consumption by Devices

| Particular | Rating (W) | Quantity | Load Rating (W) | Hours of Working (h) | Energy Rating (Wh) |
|---|---|---|---|---|---|
| Reactor | 4500 | 1 | 4500 | 2 | 9000 |
| Fan | 24 | 1 | 24 | 5 | 120 |
| Pump | 18 | 1 | 18 | 5 | 90 |
| Total | | 3 | 4542 | | 9210 |

We can see that the pump and fan must be run for more time than the reactor. This is because there will be gases escaping from the reactor up to 3-4 hours after the particular batch run has been completed. The pump will be needed to cool the gases to extract bio-oil and the fan will be required to vent uncondensed gases into the atmosphere, albeit far from human contact.

### *B. Inverter and Charge Controller Selection*

Since this is an experimental PV system setup, the desired features of the inverter are (i)Wide range of input DC voltages from the solar array, (ii)High efficiency (90+%), (iii)Single-phase pure sine wave output & (iv)Sufficient protection from overload and short circuit of Single-phase.

Similarly, desired characters of the charge controller are: (i) MPPT control, (ii) compatible with both, li-ion (CC-CV charging) and Lead-acid (bulk float charging) batteries, (iii) overcharge and over-discharge protection.

Additionally, both should have some sort of communication protocol such that they can be constantly monitored by an operator and generate data for future research and optimization of the system. These features may be skipped in large-scale plants to reduce costs.

For the above requirements, several locally available OEM PCUs from companies like Sun Power, Microtek, and Luminous were considered. These PCUs have integrated inverters and charge controllers in one compact, safe and convenient package. Although they cost more, it is justified by the flexibility offered by the system for further experimentation.

The 5 kW PCU offering from Microtek was chosen as it satisfies all the above requirements while additionally providing a hybrid solution to draw power from the grid if solar power is insufficient to drive the load.[5]

### *C. Solar Panel Selection*

Solar panels were selected after an exhaustive market research for locally available economic options. This study provided the conclusion that the two most common types available are Monocrystalline and Polycrystalline while Thin-film cell technology is currently not available easily on the market due to its high cost and low efficiency.

TABLE III
Summary of Market Research for Solar Panels

| Brand | Type | Vmpp | Impp | Power rating | Length | Width | Area | Power/area | Unit cost | Cost/watt |
|---|---|---|---|---|---|---|---|---|---|---|
| | | V | I | W | m | m | m^2 | W/m^2 | ₹ | ₹/W |
| Loom | Mono | 20.4 | 6.13 | 125 | 1.02 | 0.665 | 0.6783 | 184.28424 | 5500 | 44 |
| Loom | Mono | 19.95 | 9.03 | 180 | 1.49 | 0.665 | 0.99085 | 181.6622092 | 8000 | 44.44444444 |
| Loom | Mono | 39 | 9.75 | 380 | 1.994 | 1.002 | 1.997988 | 190.1913325 | 15000 | 39.47368421 |
| Loom | Mono | 42 | 10.5 | 441 | 2.063 | 1.026 | 2.116638 | 208.3492784 | 18000 | 40.81632653 |
| Goldigreen | Poly | 36.6 | 8.2 | 300 | 1.955 | 0.99 | 1.93545 | 155.0027125 | 7800 | 26 |
| Canadian PV | Poly | 36.8 | 8.69 | 320 | 1.972 | 0.996 | 1.964112 | 162.9234993 | 8640 | 27 |
| Waaree | Poly | 36.8 | 8.7 | 320 | 1.96 | 0.99 | 1.9404 | 164.9144506 | 8640 | 27 |
| Vikram solar | Poly | 37.7 | 8.5 | 320 | 1.956 | 0.992 | 1.940352 | 164.9185302 | 8500 | 26.5625 |
| Polycab | Poly | 37.25 | 8.6 | 320 | 1.96 | 0.989 | 1.93844 | 165.0811993 | 7900 | 24.6875 |

Mono-crystalline panels offer up to 20% advantage in specific power (W/m^2). However, this is accompanied by a cost increase of roughly 76% as compared to Poly-crystalline panels as can be seen from Table II above.

With these considerations, the Polycab PIL 320HP panel was chosen for its low cost and moderate specific power.

The TDS [6], however, provides data for test conditions under the AM1.5(Air mass 1.5) spectrum, and voltage, current, and power will vary with irradiance and temperature throughout the year and even during the day. These variations will be handled by the MPPT charge controller, which loads the solar array such that they operate at their maximum power.

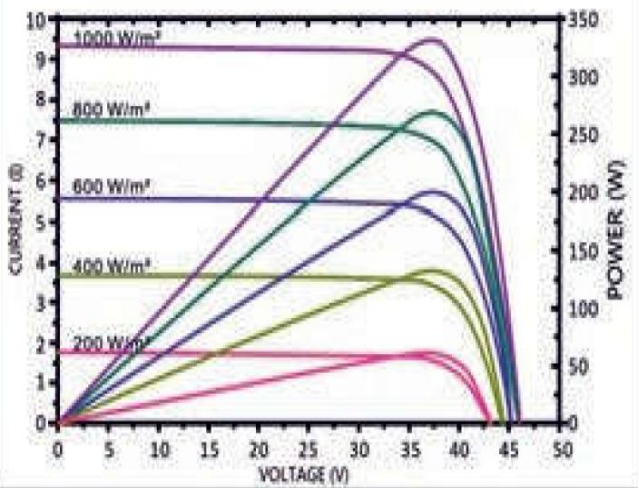


Fig. 4: I-V characteristics of solar panel [6]

*D. Solar Array Analysis*

Now that inverter and solar panels (OEM components) have been selected, array sizing can be done. Considering Polycab PIL 320 HP,

TABLE IIIII
Input Values for Array Sizing [6]

| Parameter | Value | Unit |
|---|---|---|
| Vmpp | 37.25 | V |
| Impp | 8.6 | A |
| Pmpp | 320 | W |
| Efficiency | 16.51 | % |

To operate the system at a higher efficiency, the current should be minimized. Therefore, the voltage of the DC array must be maximized within the input range of the PCU. The input DC voltage range for the PCU is 120-430V. To avoid power clipping during peak sunlight hours, the voltage of the array must be kept at 360-370V

TABLE IVV
Array Sizing Calculations

| Parameter | Formula | Value | Unit |
|---|---|---|---|
| Number of panels in series (Ns) | *Desired System Voltage/Vmpp of panel* | 9.93 ≈10 | |
| Required current capacity of the solar array | *energy rating nominal system voltage*approximate system efficiency* | 35.31 | Ah |
| Current generated by the solar array | *Current capacity/ESH (Taking ESH=5 hours)* | 7.06 | A |
| Required power | *Current * system voltage* | 2629 | W |

Since Im(panel)= 8.6A > current requirement from the solar array,
Number of parallel strings (Np) = 1
At maximum power point, the array specifications will be:

TABLE V
SOLAR ARRAY SIZING RESULTS

| Parameter | Formula | Value | Unit |
|---|---|---|---|
| Vmpp(Array) | *VmppPanel * Ns* | 372.5 | V |
| Impp(Array) | | 8.6 | A |
| Pmpp(Array) | *PmppPanel*Ns * Np* | 3200 | W |

*E. Site Survey*

Since solar energy is highly dependent on the conditions of the installation location, a site survey is essential for a well-designed system.

In this case, the identified site of installation is the roof of the "Aryabhatta" building of KJ Somaiya College of Engineering.


Fig. 5: a) Solar array placement at the site and b) Close-up of the solar array (Helioscope and google maps)

The site features a roof roughly 50mx50m in size with plenty of un-shaded areas with no trees, poles, or buildings which will allow for uninterrupted and efficient conversion.

It can be seen from fig. 5, that the array will occupy a maximum of 42.63 m2. The location of the site is (Courtesy: GOOGLE maps): Latitude: 19.0727 °N, Longitude: 72.8999 °E. The site receives about 4-5kWh/m2 of solar energy per day.

With sufficient unshaded area with plenty incident solar energy throughout the year, the identified site is suitable for installation of a solar photovoltaic system.

*F. Direction and Tilt*

Since this is a pilot project, the aim was to keep the system simple. Thus, solar tracking has not been discussed or implemented as it adds complexity with only as much as 3-5% gain in efficiency. The array is designed for a fixed azimuth and fixed tilt angle.

The Azimuth of the solar array is defined as the orientation of the solar panels. It is measured in degrees, with the North taken as 0° and the South as 180°. For the northern hemisphere, as a rule of thumb, a good place to orient the solar panels is directly South. This is affirmed by an azimuth angle optimization study using PVSyst software discussed in later chapters.

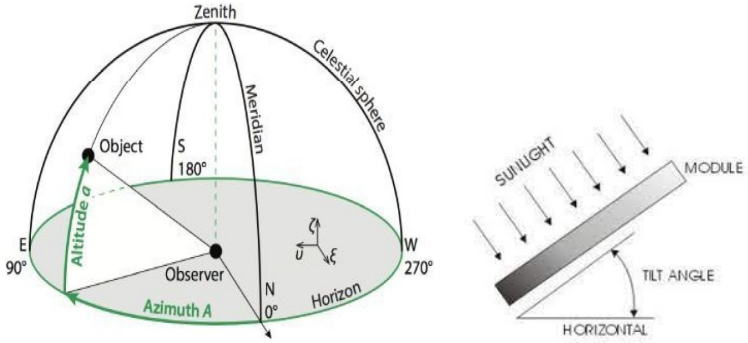


Fig. 6: Illustration of various solar angles [7]

The Tilt of the solar panel is the angle they are installed measured from the horizontal. A good approximation of tilt can be simple to use the latitude of the location as the angle of tilt. However, this may not always be true. Therefore, historical data is used for the approximation of tilt angle.

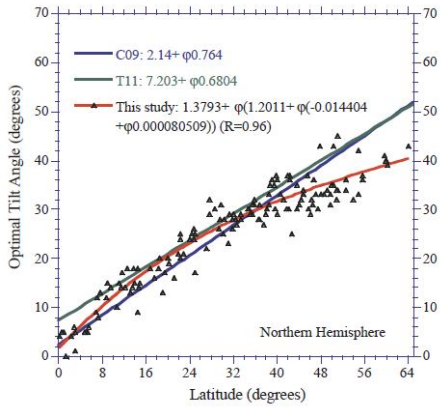


Fig. 7: Historical data of optimal tilt angle vs latitude.[8]

Observing the plot of optimum tilt angle vs latitude for historical data from all around the world, the curve fitting of the data gives the following equation.

Optimal tilt angle $\theta = 1.3793 + \phi\ (1.2011 + \phi\ (-0.014404 + \phi\ (0.0000805090))$; where $\phi$=location latitude.

For site location, $\phi = 19°$ N, substituting $\phi$ we can get $\theta = 19.55256 \sim 20°$.

| Paticular | Rating (W) | Quantity | Load Rating (W) | Hours of Working (h) | Energy Rating (Wh) |
|---|---|---|---|---|---|
| Pyrolysis setup | 4500 | 1 | 4500 | 2 | 9000 |
| Fan | 24 | 1 | 24 | 5 | 120 |
| Pump | 18 | 1 | 18 | 5 | 90 |
| Total | | 3 | 4542 | 12 | 9210 |

| | | | | | |
|---|---|---|---|---|---|
| **Required capacity (Ah)** | 24.7580645 | Ah | **Required power (W)** | 1842 | W |
| **Required capacity (Ah) considering System efficiency** | 35.3686636 | Ah | **Required power (W) considering System efficiency** | 2631.428571 | W |
| **Current generated (A)** | 7.07373272 | A | | | |
| | | | **Optimum fixed tilt angle** | 19.55256723 | ° from horizontal |
| **Number of modules in series (Ns)** | 10 | | **Winter optimum fixed angle** | 34.55256723 | ° from horizontal |
| **Number of modules in Parallel (Np)** | 1 | | **Summer optimum tilt angle** | 4.552567231 | ° from horizontal |
| **Total** | 10 | | | | |
| | | | **Circuit breaker rating** | 8.6 | A |
| **Total PV power** | 3203.5 | W | | | |

| | | |
|---|---|---|
| **Nominal System Voltage** | 372 | V |
| **System Efiiciency** | 0.7 | |
| **Equivalent Sun Hours (ESH)** | 5 | Hours |
| **PV module voltage** | 37.25 | V |
| **PV module current rating** | 8.6 | A |
| **PV module power rating** | 320.35 | W |
| **Latitude of installation site** | 19 | ° |

Fig. 8: Solar Array Calculator Spreadsheet

Thus, for the selected site, the optimum all year angle is determined as 20°

*G. Wind Force Calculation and Simulation*

Wind force calculation is done using formulae for the jet incident on an inclined plate.

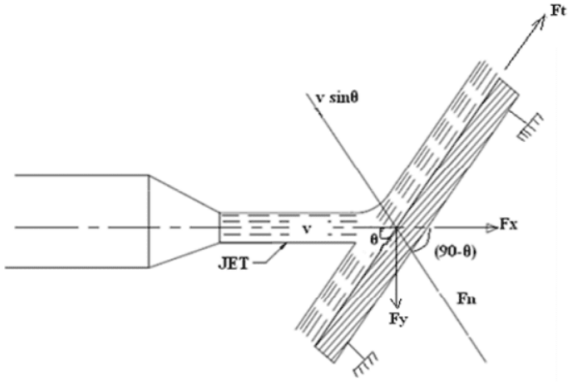


Fig. 9: Impact of jet on a flat inclined plate.

Density of air ρ=1.225kg/m3
Length of panel (l) =1.96m; Width of panel (b) = 0.989m
Area of panel (A)= l*b = 1.938m2
Let θ be the angle of the panel with respect to the horizontal,
θ =20°……. Angle of tilt determined earlier.
V=15m/s……. Average speed of monsoon winds in Mumbai.
Normal force,
Fn =ρ*A*V^2*sinθ =1.225*1.938*152xsin20°=182.7353858 N
Force in the x-direction,
Fx=Fn*sinθ=182.7353858*sin(20°) = 62.49918283N
Force in the y-direction,
Fy=Fn*cosθ=182.7353858*cos (20°) = 171.7150936N

TABLE VI
Wind Forces Acting on Solar Panels

| | | |
|---|---|---|
| Fn | 182.735 | N |
| Fx (horizontal) | 62.4992 | N |
| Fy (vertical) | 171.715 | N |

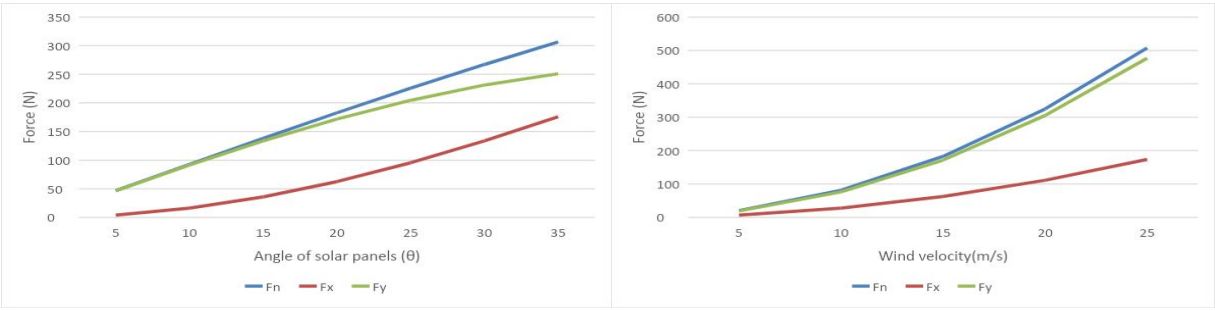


Fig. 10: a) Variation of forces was plotted with respect to wind velocity at a fixed angle of 20°; b) Variation of forces was also plotted against the angle of inclination with a fixed wind speed of 15m/s.

Additionally, CFD analysis was performed to obtain forces exerted on the panel by 15m/s wind at 20° angle of inclination with the wind in both, forward and rear direction. The simulation was carried out on SIMSCALE.

1) *Geometry Preparation:* The geometry consists of a plate of the representative dimensions of the solar panels, inclined at 20° to the horizontal. The enclosure is 14m in length, 10m in width, and 5m in height. The enclosure is sized to give sufficient room for the flow to develop properly before being incident on the panel as well as after the interaction. The software automatically creates contacts and there is no need for additional contact definition.
2) *Boundary Conditions:* Velocity inlet is given at the desired wind direction and 15m/s inlet velocity. The floor, which needs to simulate the ground, is made a no-slip wall. All other faces are pressure outlets set at 1 atm.
3) *Mesh Details:* Hex dominant mesh was used for the simulation. Mesh sizing was set to automatic. The boundary layer number was set to 3 with a 1.5 growth rate. Number of cells: 376,100; Number of nodes: 134,400
4) *Results*

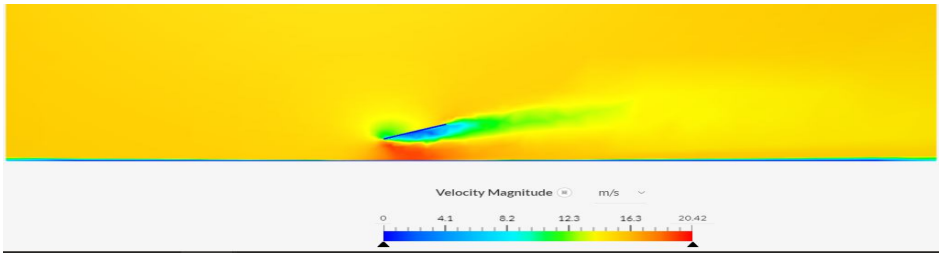


Fig. 11: Velocity plot of flow. Wind from the front of the panel.

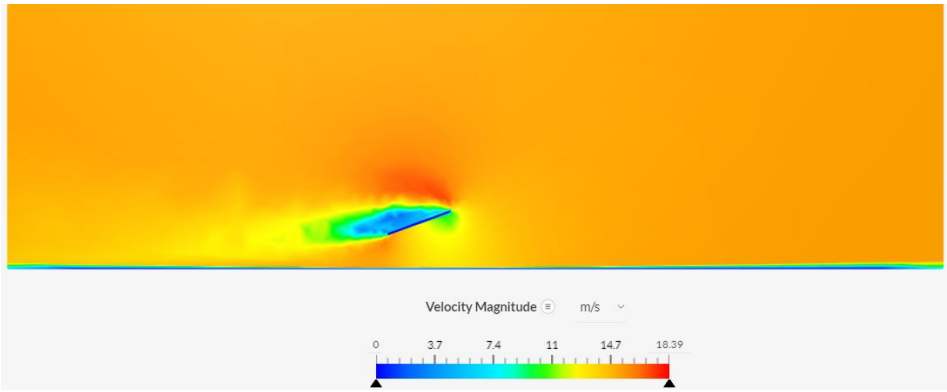


Fig. 12: Velocity plot of flow. Wind from the rear of the panel.

From the simulation results, the forces acting on the solar panels can be summarized in Table VII below. The force data can be used to design sturdier and more optimized mounting structures depending on prevailing conditions at the site of installation.

TABLE VII
Wind Forces Acting on Solar Panels from CFD Study

| Direction of wind | Fx (N) | Fy (N) |
|---|---|---|
| Front | 133.24 | 318.45 (downward) |
| Rear | 113.44 | 267.92 (upward) |

The difference between the calculated and simulated values of force could be attributed to the simple model used for the analytical calculations while the simulation takes into account skin friction, pressure forces etc.

*H. Solar Panel Mount Design*

Since the solar array will constantly be exposed to the elements, a non-corrosive material is a passive or passivized material. Due to the sunlight and wind exposure, most externally applied coatings like powder coat or paint will gradually result in pitting corrosion before being stripped away altogether. Thus, stainless steel and anodized aluminum were considered for the mounting structure.

*1)* Aluminum is expensive and has lower strength values, it has the advantage of being light, but that does not count for much in this case. Anodizing process must be done after welding, resulting in additional cost.

*2)* Stainless steel is 1/3rd the cost of aluminum and is naturally passive due to its chromium content.

Thus, stainless steel SS304 was chosen as the material for the mounting structure.

A CAD model of the solar panel was prepared according to the drawing of the manufacturer, and the mounting structure was modelled.

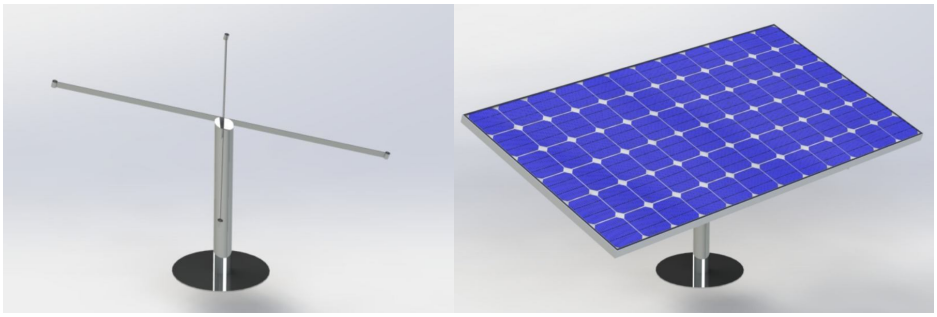

Fig. 13: a) CAD rendering of Stainless-steel mounting structure; b) CAD rendering of solar panel mounted on the structure

The solar panel will be mounted using 4x M6 bolts and nuts to this stainless-steel structure. The mounting structure is of a fixed angle design for the sake of simplicity. Further iterations can be done to add functionality such as adjustable angles and 1 or 2 axis solar trackers.

*ISSN: 2321-9653; IC Value: 45.98; SJ Impact Factor: 7.429*
*Volume 9 Issue IX Sep 2021- Available at www.ijraset.com*

## III.ENERGY STORAGE SYSTEM DESIGN

The storage system of a PV plant has the function of storing excess energy and releasing the energy stored for use when the output from the solar array is low or zero. This can be used to power loads at night and during days with high cloud cover and at night.
For this project, we have chosen to design a chemical storage system due to its flexibility, high efficiency, and absence of moving parts as opposed to flywheel storage pumped hydro or other mechanical storage systems.

The preliminary calculations can be done as below:
Battery voltage VB is 48V as specified in the TDS of the PCU [5]. Assuming battery backup time required is 1 day, the initial estimation of energy required is 9.21kWh. For further calculations, Cell chemistry must be chosen first such that calculation inputs are appropriate.

### *A. Cell Chemistry Selection*

There are many types of chemical batteries classified based on the chemical makeup of the active ingredients. For the scope of this project, cell chemistries of secondary cells that are commonly available are compared.

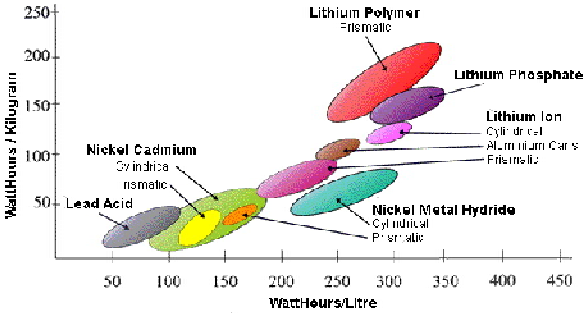


Fig. 14: Ragone plot for cell chemistry comparison (University of Oregon)

We can eliminate Nickel-Cadmium (NI-Cd) batteries due to the toxic nature of cadmium. Nickel metal hydride (NiMH) batteries can be eliminated on the grounds of availability since they are available only in small formats in India. Both Ni-Cd and NiMH batteries suffer from memory effects when charged and discharged partially.

This leaves us with lead-acid and lithium-based cells, which are, as of today, the most used chemical batteries.

| | Lead Acid | Li-ion |
|---|---|---|
| Nominal cell voltage | 2V | 2.5V/3.3V/3.6-3.7V |
| Specific Energy | 30-45 Wh/kg | 90-220 Wh/kg |
| Energy Density | 60-75 Wh/L | 280-400 Wh/L |
| Specific power | 180 W/kg | 600-3400 W/kg |
| Cycle life | 500-800 | 1000-8000 |
| Self-discharge | 2-45% /month | 2-5% /month |
| Temperature range | -20-60°C | -20-60°C |
| Relative costs | Low | High |

Fig. 15: Comparison of Li-ion and Lead-acid batteries [9]

From table viii, we can observe that li-ion batteries are better in almost every aspect. The only place where lead-acid batteries have the edge is that they are a mature technology that costs much less and are much safer than li-ion batteries. This is the reason why they are so commonly used in domestic solar applications. Lead-acid technology has matured and is unlikely to make significant progress soon.
Lead-acid batteries have low efficiency, a high rate of self-discharge, and a low Depth of Discharge (DoD) to maintain cycle life. If DoD is increased, cycle life drops severely. For example, lead-acid batteries are rated at about 2000-3000 cycles for a 40% depth of discharge at C/10 current, while LiFePO4 batteries are rated at 2000-3000 cycles for 80% DoD at C/5 discharge rate. This will require a severe oversizing of the battery to meet our requirements and would quickly become unviable for upgradation to a larger scale.
Li-ion batteries are gaining momentum as viable chemical batteries for solar energy. This application is a good chance to study the behaviour of Li-ion batteries. Thus, li-ion batteries were chosen as the chemical storage battery for this project.

There are many variants in li-ion batteries as well, based on electrode chemistry, some of which are illustrated in the figure below.

| Chemistry | Chemistry Abbre-viation | Typical Voltage | Specific Energy (Capacity) | Cycle Life | Charge (C Rate) | Discharge (C Rate) | Durability in High Temp. Environments | Thermal Runaway Temp. | Production Costs |
|---|---|---|---|---|---|---|---|---|---|
| Lithium Cobalt Oxide (LiCoO22) | LCO | 3.7 V | 150-200 Wh/Kg | 500-1,000 | 0.7-1.0C, charges to 4.20V | 1C; 2.50V cut off | Low | 150°C (302°F) | Low |
| Lithium Manganese Oxide (LiMn2O4) | LMO | 3.7 V | 100-150 Wh/Kg | 300-700 | 0.7-1.0C typical, 3C max.; charges to 4.20V | 1C typical; 10C on some cells; 2.50V cut off | Low | 250°C (480°F) | Low |
| Lithium Nickel Manganese Cobalt Oxide (LiNiMnCoO2) | NMC | 3.6 V | 150-200 Wh/Kg | 1,000-2,000 | 0.7-1.0C, charges to 4.20V | 1C bypical; 2C on some cells; 2.50V cut off | Low | 210°C (410°F) | Low |
| Lithium Nickel Cobalt Aluminum Oxide (LiNiCoAlO2) | NCA | 3.6 V | 155-260 Wh/Kg | 500 | 0.7C, charges to 4.20V | 1C typical; 3.00V cut off | Low | 150°C (302°F) | Medium |
| Lithium Iron Phosphate (LiFePO4) | LFP | 3.2 V | 90-125 Wh/Kg | 1,000-3,000 | C/2 to 4C, charges to 3.7V | 1C typical; 30C on some cells; 2.50V cut off | High | 270°C (518°F) | Low |

Fig. 16: Lithium-ion (Li-Ion) technology comparison. (a)LCO; (b)LMO; (c)NMC; (d)NCA; (e)LFP [9]

From fig. 17, we can observe that LFP or Lithium Iron Phosphate batteries turn out to be one of the best combinations of safety and performance. They are also one of the few li-ion chemistry batteries readily available in India.
For this reason, LFP batteries were finalized as the choice of chemistry for the project.

*B. Cell Format Selection*

LFP batteries are commonly available in three formats, namely: cylindrical, pouch, and prismatic.

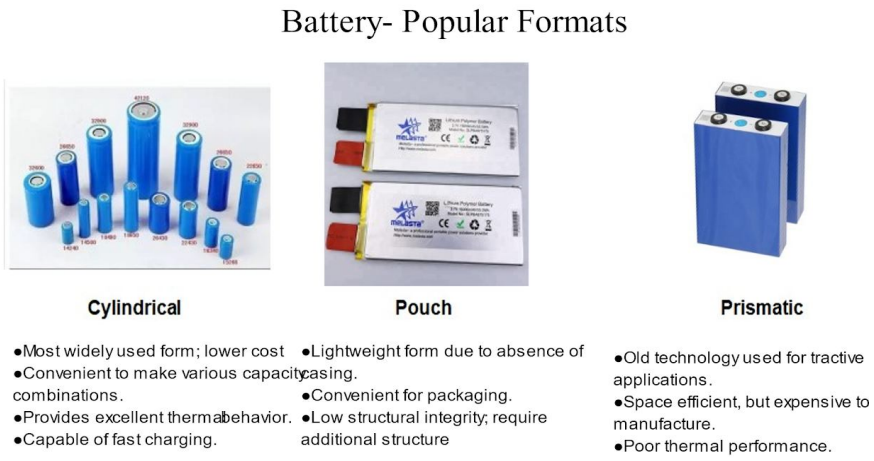


Fig. 17: Comparison of various battery formats.

Cylindrical cells consist of active ingredients (commonly known as 'jelly rolls') packed in small steel or aluminum cans. They have the advantage of good thermal properties and modularity, but they require large numbers of cells connected in series and parallel to make any sizable battery pack. While Pouch cells are light and easy to package, they need extensive protection structures due to their soft structure. Prismatic cells are available in large formats up to around 300Ah, greatly reducing the number of cells required to make a big battery pack. They are also commonly available in India at a relatively low cost. Hence, a prismatic format was chosen for this project.
The energy required to run the reactor for one day = 9.21kWh. Assuming 80% DoD,
Energy capacity required = Required battery capacity/DoD =92100.8=11512.5 Wh~11.512kWh
Current capacity required = Actual energy required/Battery nominal voltage=11512.5/48=239.84Ah
According to market research, the best configuration for this capacity would be a 120Ah cell with 2 parallel strings to get 240Ah current capacity.

| | |
|---|---|
| Model No. | L173F120 |
| Nominal Capacity | 120Ah |
| Nominal Voltage | 3.2V |
| Impedance | 0.2~0.3mΩ |
| Dimension | 49*173*165mm |
| Standard Charge Current | 24A |
| Standard discharge current | 120A(max.3C) |
| Max.charge voltage | 3.65V |
| Discharge cut-off voltage | 2.5V |
| Charge method | CC/CV |
| Charge working temp. | 0~45 ℃ |
| Discharge working temp. | -20~55 ℃ |
| Cycle life | >2500 cycles |
| Battery Weight About | 2.9KG |

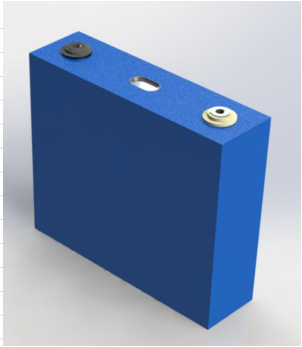

Fig. 18: a) Datasheet of selected Cell, b) CAD rendering of the selected cell

Number of cells in series (Ns) = Battery pack voltage/Nominal voltage of single cell=48/3.2= 15
Number of cells in parallel (Np) = Current capacity required /Current capacity of single cell=239.84/120=1.998~2
Thus, 30 of these large format cells would be needed to be connected in 2p15s configuration to create the desired battery pack.

*C. Battery Thermal Calculations and Simulation*

Since the cell is made of various materials in proprietary combinations, general lumped properties of similar cells are taken (Lumped specific heat Cp=1.067 kJ/kg K, thermal conductivity= 20W/mK, m=2.9kg, internal resistance (Rint)=0.0003ohm[10].
Now, the current flowing through the battery pack is being discharged at 4.5kW
I= Power drawn/Battery Voltage=4542/48=92.62A
Since the battery configuration is 2 parallel strings,
Icell=I/2=92.622=47.31A
Thus, assuming heating is only due to the internal resistance of the battery, applying the Joule heating principle,
Power lost due to heating (P)= I^2*Rint =47.312*0.0003 =0.6714W
Assuming the setup is run continuously for 2 hours,
Heat energy lost E=P*time=0.6714*2*3600=4832.08J
Thermal inertia of the cell = m*Cp=2.9*1067=3092.3J/K
Assuming all the heat lost is stored in the cell,
Temperature rise ΔT= E/(m*Cp) =4832.08/3092.30=1.56°C
Since the temperature rise of the battery is 1.56°C from ambient temperature, which is well within the temperatures suitable to the particular battery, the design is safe and does not require any active cooling provision.
Lumped steady-state thermal simulation was carried out on SIMSCALE software using the CHT (Conjugate Heat Transfer method). Properties of the cell were taken from the earlier thermal calculations chapter. The simulation was carried out for 7200s which is the designed operating period.

1) *Boundary Conditions:* To simulate a closed battery box of 1m x 1m x 1m enclosure, all surfaces of the enclosure have been assigned as no-slip walls. Heat input of 1.14W, which is 50% greater than the actual heat power lost. This is to compensate for the effects of contact resistance on the heating. The air in the enclosure had an initialized temperature of 25°C or 298K.
2) *Results*

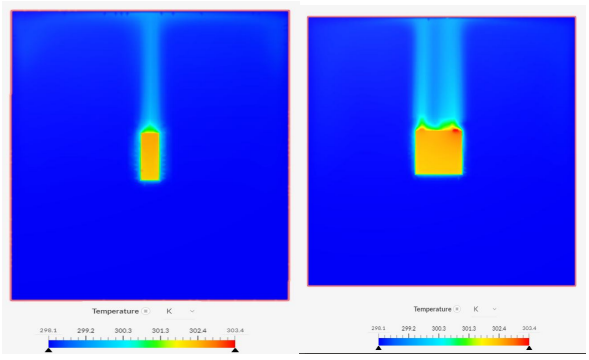

Fig. 19: Temperature distribution (side view section & front view respectively)

From the simulation results in Fig. 20,21, a maximum temperature of 303.4K or 30.4°C can be observed from an initial temperature of 25°C which gives a temperature rise of 5.4°C. In the previous chapter, the temperature rise of 1.56°C had been obtained from hand calculations. The discrepancy arises because the numerical analysis did not consider the local rise in temperature. For instance, maximum heat is evolved at the negative terminal of the cell because the corresponding electrode is generally made of graphite which offers more resistance to electron flow.

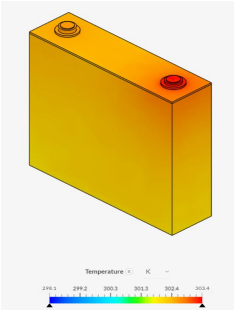

Fig. 20: Temperature distribution on the cell surface

*D. Battery Module Design*

Since the battery is inherently very heavy, it must be split into modules for ease of assembly, maintenance, and overhaul. They must also be divided so that the probability of thermal runaway can be reduced. Since the pack configuration is 2p15s, consisting of 30 cells in total, it can be split into 5 equal segments of 2p3s configuration each.

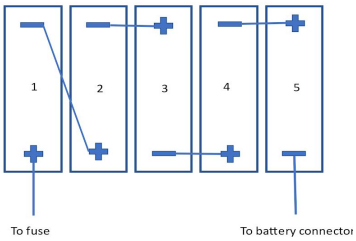


Fig. 21: Battery connection diagram.

For the connection of modules 1 and 2, to prevent wrong connection and fool-proof the connection, an appropriate combination of male and female connectors shall be used.

*E. Battery Structures*

The modules must be given a suitable structure with the following characteristics:

a) Must be strong enough to sustain the weight of the module; b) Must be non-conductive to prevent leakage current issues and c) Must be easy to lift since the module will be significantly heavy. The battery and its complementary components must be housed in a non-conductive metal housing to protect the battery from harm as well as the people in case of a mishap.

For the module structure, aluminum was chosen due to its ability to be passivized using anodizing, thus forming an insulating layer around the metal. It is also strong enough to easily support the weight of the module.

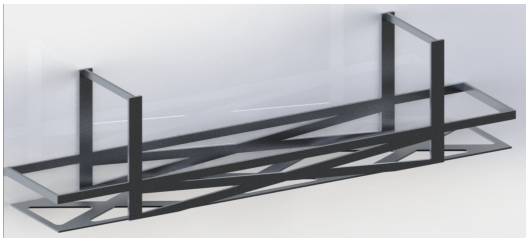

Fig. 22: CAD rendering of battery module structure.

The module structure shall be constructed from 3mm thick anodized aluminum alloy Al6061-T6 for its high strength properties. The plates shall be cut into shape using the waterjet cutting process for higher accuracy and welded together using a suitable fixture.

*F. Structural Analysis*

Static structural analysis was carried out to find out the structural soundness of the design.

Material properties: Al6061-T6, density ρ=2700kg/m3, Youngs modulus = 69 GPa, tensile yield strength = 275 MPa & tensile ultimate strength = 310Mpa.

*1) Boundary Conditions*

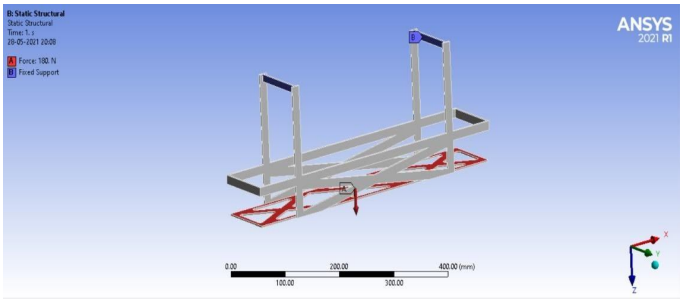


Fig. 23: Boundary conditions of the analysis.

Fixed support was provided to the handles provided for lifting. To simulate the forces acting on the cell module, only the weight of the cells, busbars, wires and connectors were applied as a force to the structure (assuming there will be no other significant forces due to the static nature of the application). Total weight in one module was estimated as 18 kg. Force was applied to the lower plate that supports the cells, the magnitude of which is (Assuming gravitational acceleration g =9.81m/s2) F = m*g = 18*9.81 = 176.58 ~180N.

*2) Results*

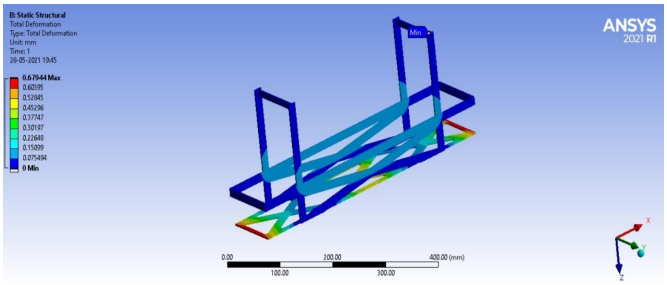


Fig. 24: Total deformation

The maximum deformation is at the unsupported base plate edges at 0.67mm. This does not cause loss of function and should be safe.

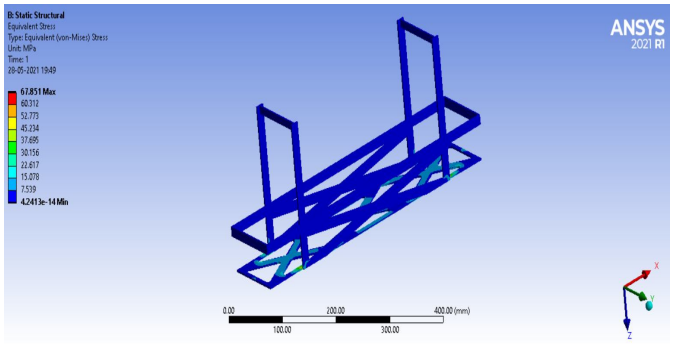


Fig. 25: Maximum equivalent stress

The maximum stress calculated is 67.87 MPa which is well under the yield stress of the material (250MPa).

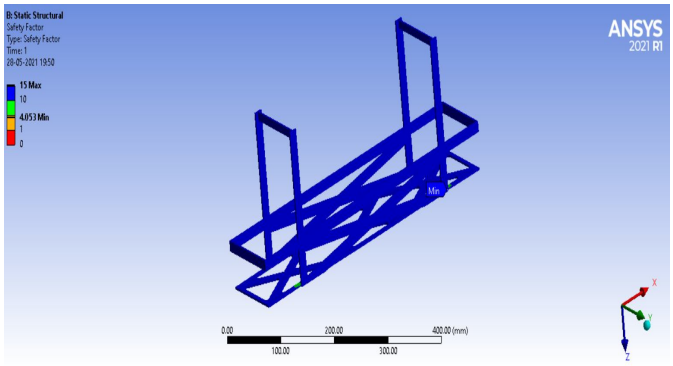


Fig. 26: Factor of safety

The lowest factor of safety observed was 2.053 at the points where the handlebars meet the base. This shows that there is a stress concentration point where the flow of stress in the structure is present. However, this can be overlooked for this case since there is no fatigue loading of the component. Keeping this in mind, the structure is deemed safe for use.

*G. Busbar Design*

The busbars are used to make the series and parallel connections within the module. They must have the following characteristics: i) Non-corrosive to prevent high contact resistance; ii) High conductivity and iii) High specific heat capacity to store heat generated effectively. Copper and aluminum were compared for this application. However, aluminum was chosen due to its high specific heat and high conductivity. The corrosive properties of copper could be eliminated by using tin-plated copper. This can be studied for future applications.

Busbar cross-section was selected from data provided by the Electrical Power Engineering: Reference & Applications Handbook [11].

Table VIII
Current Ratings for Rectangular Cross Section (Grade EIE-M (1350)) [11]

| *Cross-sectional area (mm^2)* | *1 bar* |
|---|---|
| 30 | 118 |
| 40 | 151 |
| 50 | 183 |
| 62.5 | 223 |
| 75 | 263 |
| 100 | 342 |

Since the current being drawn is about 100A continuously for 2 hours, the busbars cross-section was chosen to be 75mm2, rated at 263A continuous. This was done to keep the heating to a minimum and compensate for unaccounted heating from contact resistance.

The series connection busbars are split into two sections of 37.5mm2 to allow for the connection of 2 cells in parallel. The 2 series busbars are connected in parallel using a thin aluminum strip that will serve as the parallel fuse to disconnect the two parallel strings in case there is an internal short circuit in the cell or if one cell starts charging the other due to a voltage imbalance.

For fusing current calculations, the cell is rated at 3C or 360A current for 10-second bursts. The fusing section is designed to blow at a current of 480A in 10 seconds.

From CAD, the thickness of busbar t = 3mm, the width of busbar w = 2mm, Length of busbar l = 30mm, area of cross-section, ambient temperature = 35°C & fusing time = 10 s

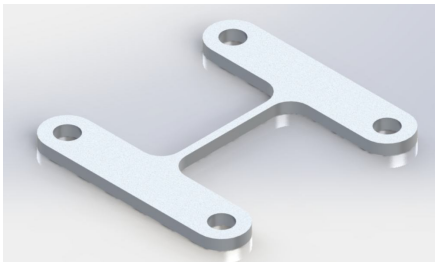

Fig. 27: CAD rendering of Aluminum busbar used to make series and parallel connections.

The properties of aluminum are resistivity =2.65E-8 ohm.m, density = 2700 kg/m3, Cp = 910 J/kgK & melting point = 660°C.
Resistance R=ρ*l*A=1.33E-04 ohm
Heat output (P)=I^2*R=4802x1.33x10-4= 30.53W
Heat energy (E)= P*time=30.53x10=305.3J
Mass of fusing section m =density * volume=0.0004878kg
Temperature rise ΔT= E/ (m* Cp) =305.3/(0.0004878 x 910)= 687.725558
Final temperature = 687.725558+35 = 722.7255586 °C.
This is greater than the melting point for aluminum. Thus, this link will fuse if 480A for 10s pass through it.

TABLE IX
Calculation Output for Fusing Section

| | | | | | |
|---|---|---|---|---|---|
| Average current | 480 | A | Heat output | 3.05E+01 | W |
| | | | | 305.28 | j |
| Width of bus | 2 | mm | | | |
| Thickness of bus | 3 | mm | Mass of one busbar | 0.000488 | kg |
| Length of busbar | 30 | mm | M*Cp | 0.443898 | |
| Ambient temp | 35 | °C | Temp rise | 687.7256 | °C |
| Run time | 10 | s | Final temp | 722.7256 | °C |
| Resistance | 1.33E-04 | ohm | | | |

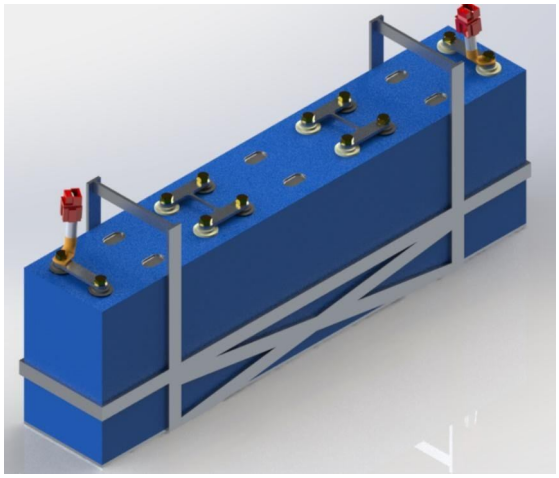

Fig. 28: CAD rendering of the battery module.

In Fig. 29 above, it can be seen that the connections are made by the aluminum busbars bolted onto the cells using brass bolts. At the terminals, a connector crimped onto 25mm2 cables, used to make inter-module connections are attached with the help of a cable lug and a brass bolt.

*H. Battery Housing Design and Insulation*

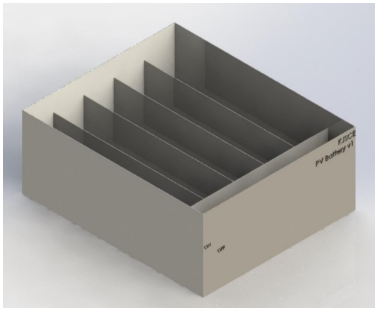

Fig. 29: CAD rendering of battery container

The battery housing consists of a box made with 1.5mm thick stainless steel welded together, that has been provided with compartments for the five modules.
The inner walls of the box are lined with Nomex® paper to provide insulation and additional flame retardance to the container, contributing to its safety.

*I. Additional Components*

1) *Cables:* Cables were selected from the manufacturer datasheet. These are single-core DC cables rated at 1000v and a max operating temperature of 120°C. Cables of 6mm2 were chosen for the solar array side. Although these cables are rated for 70A, which is almost 10 times the current of the array at the maximum power point, they were chosen to keep losses to a minimum and temperatures within manufacturer limits. Cables of 25mm2 were chosen for the battery application. These are rated at 176A and should be future-proof for upgrades.
2) *Safety devices:* Fuses or MCBs are interrupting devices that are used to protect electrical systems from overloading and damaging the components. The interrupting device used for the solar array is a 15A rated DC MCB. This rating is specified by the solar panel manufacturer. The interrupting device used for the battery system is a 150A DC fuse since the minimum rating in the system is that of the cables at 176A. It is very difficult and expensive to procure an MCB for a similar current capacity locally, thus a fuse was chosen as a suitable interrupt device. A BMS device is also required for the battery to interrupt operation if the cell temperature exceeds a certain threshold or the cells are either overcharged or over-discharged.

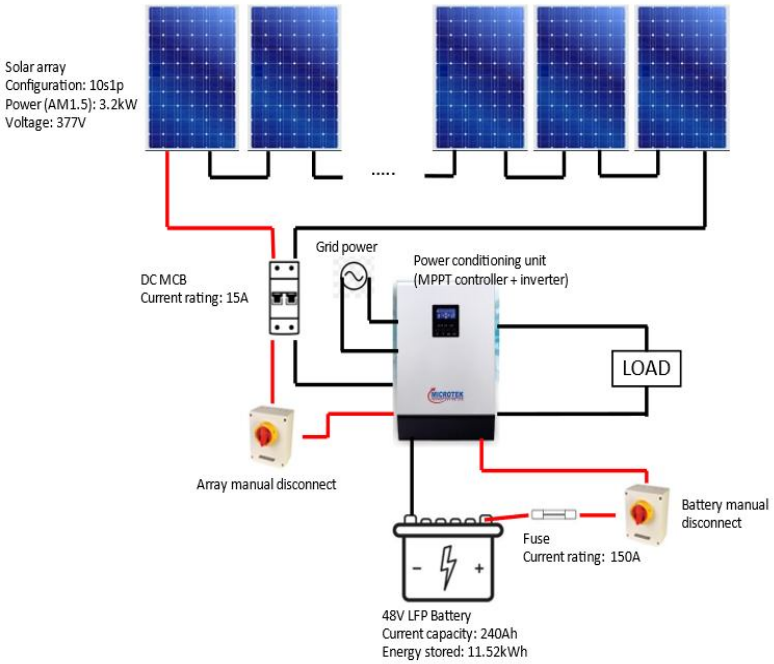


Fig. 30: Complete solar PV system connection diagram.

## IV. SYSTEM SIMULATION

The system thus designed was simulated using PVSyst software as a way of digital validation. This software is designed to simulate both on and off-grid solar PV systems.

Various irradiance databases are available within the software. From these, Meteonorm 8.0 was chosen due to its high resolution global meteorological database.

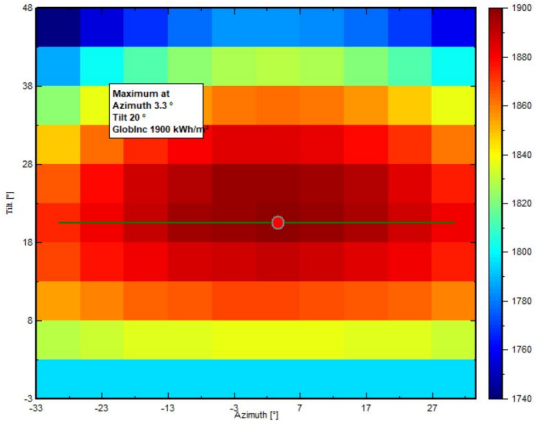


Fig. 31: Result of tilt and azimuth optimization study (To maximize incident radiation).

In the above figure, the distribution of incident energy against azimuth and tilt angle can be seen. The optimal tilt angle can thus be determined as 20° and azimuth angle as 3.3°.

**System Production**

| | | | |
|---|---|---|---|
| Available Energy | 4932 kWh/year | Specific production | 1536 kWh/kWp/year |
| Used Energy | 3275 kWh/year | Performance Ratio PR | 53.69 % |
| Excess (unused) | 1557 kWh/year | Solar Fraction SF | 97.18 % |
| **Loss of Load** | | **Battery aging (State of Wear)** | |
| Time Fraction | 2.5 % | Cycles SOW | 95.4 % |
| Missing Energy | 95 kWh/year | Static SOW | 74.5 % |

**Economic evaluation**

| Investment | | Yearly cost | | LCOE | |
|---|---|---|---|---|---|
| Global | 267'500.00 INR | Annuities | 0.00 INR/yr | Energy cost | 0.00 INR/kWh |
| Specific | 83.3 INR/Wp | Running Costs | 0.00 INR/yr | | |
| | | Payback period | 10.2 years | | |

Fig. 32: Main results summary

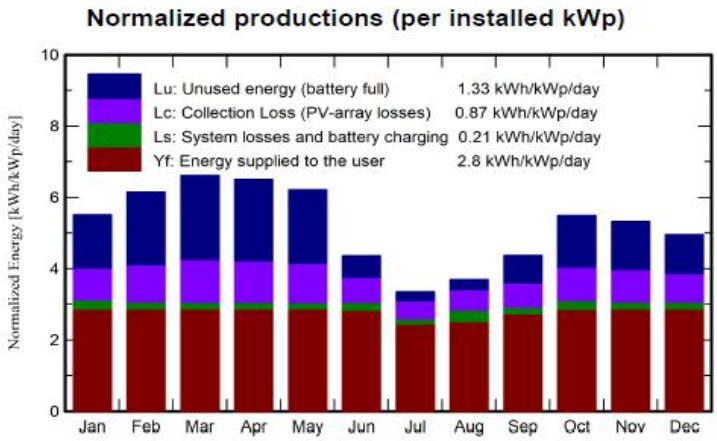


Fig. 33: Normalized production (kWh/kWp/Day)

Observing these results, it was found that the batteries were slightly undersized for all months except July (when the monsoon cloud cover would reduce incident) energy due to which, a lot of incident energy is unused as the battery is full. However, the excess energy could be used to run additional devices as per user requirements.

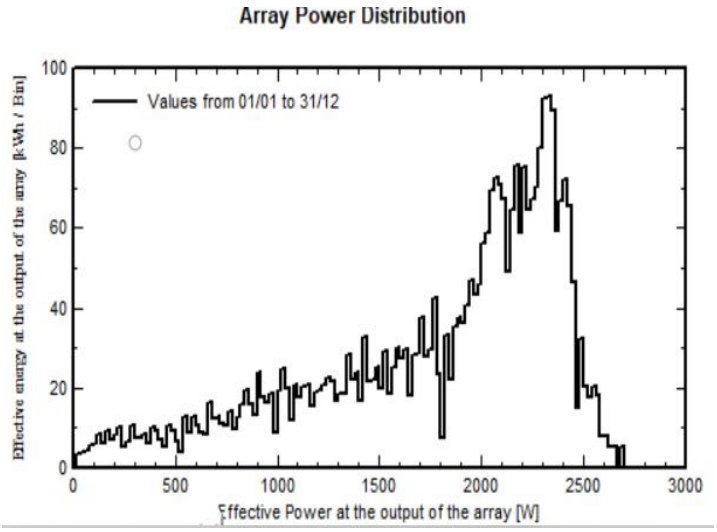


Fig. 34: Array power distribution.

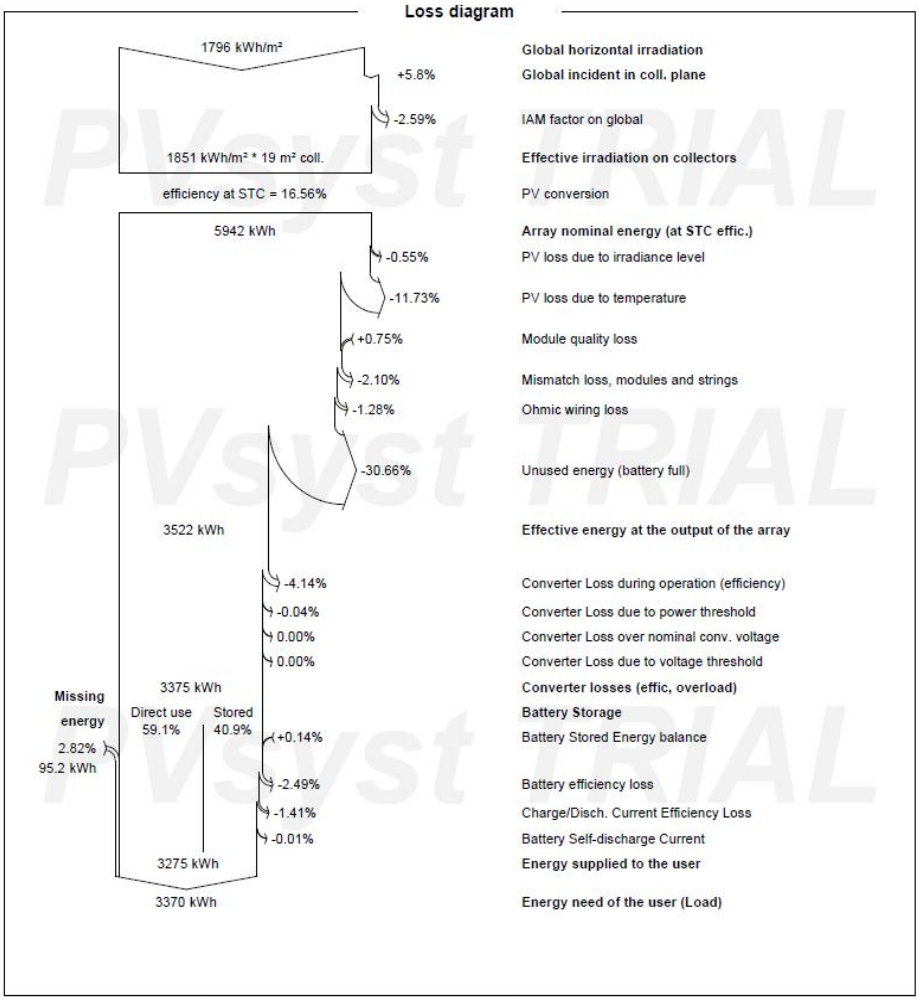


Fig. 35: Loss diagram.

From the system simulations, we can conclude that the design is sufficient for use all year long.

## V. COST ANALYSIS

The cost of Installation of the Solar photovoltaic system is summarized in the table below. The costs and availability of the various components are subject to changes technology and market trends.

TABLE X
Cost of PV Setup

| Component | Unit cost | Cost |
|---|---|---|
| Panel Polycab PIL 320HP | 7900 | ₹ 79,000.00 |
| Inverter (PCU) | 70000 | ₹ 70,000.00 |
| Battery cells | 2500 | ₹ 75,000.00 |
| Battery management system | 5000 | ₹ 10,000.00 |
| Fuse | 535 | ₹ 1,070.00 |
| Junction box | 1000 | ₹ 1,000.00 |
| MCB | 530 | ₹ 530.00 |
| Manual disconnects | 560 | ₹ 1,120.00 |
| Nomex Insulating paper | 800 | ₹ 2,400.00 |
| Polycab flame retardant 6mm^2 copper wire | 40 | ₹ 2,000.00 |
| Structure Stainless Steel, aluminum, and fabrication | | ₹ 25,000.00 |
| Total | | ₹ 267,120.00 |

### *A. Payback period of solar Photovoltaic system*

The payback period is calculated considering only cost savings due to grid independence.
Cost of electricity at site = Rs 8 per kWh
Total investment = Cost of reactor setup + Cost of solar PV system = Rs. 3,05,570
No. of operating days = 300 days per year
Average energy generated by the setup = 16 kWh per day
Cost-saving per day = No. of units generated in a day x cost per unit = Rs. 128
Cost-saving per year = Cost saving per day * No. of operating days = Rs. 38,400
Payback period = Investment/Cost savings per year = 7.95 years~ 8.00 years

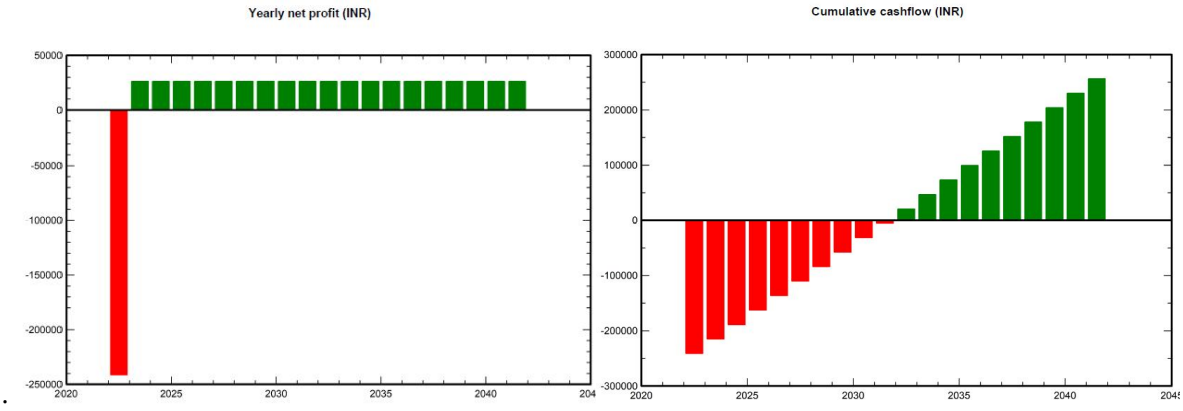


Fig. 36: a) Yearly net profit. and b) Cumulative cash-flow

Further, these financial parameters were input into PVSyst software discussed earlier which resulted in a payback period of 10.2 years and can also be observed from the cumulative cash flow chart in fig. 37b.

Moreover, Solar PV arrays cost the environment less since they produce only 30-50g of $CO_2$ per kWh, a figure that is almost 20-30 times lesser than coal or other fossil fuel fired power generation. [12]

The bio-char and bio-oil produced could be a source of additional income but they have not been considered for the purpose of this project.

## VI. CONCLUSIONS

Solar energy collection systems were studied, from which an off-grid PV system was chosen and detailed design was done for various components of the system. This system architecture was chosen due to its flexibility and reliability as well as the ability to operate in remote, non- grid-connected areas such as farms and villages where grid supply may be intermittent or unreliable.

Market research revealed Polycrystalline modules to be more viable for the project than either monocrystalline or thin-film solar cells due to their easy availability in the country and affordable nature.

For a storage system, Lithium-ion batteries were chosen for this high-power application due to their efficiency, compactness and as this is an experimental setup, the potential observations and experimentation with the Lithium-ion batteries are vast.

Costing analysis of the system revealed that with the addition of solar power, the products of pyrolysis (Biochar and bio-oil) can turn up a profit while the system pays back its initial investment in about 8-10 years, which is well within the estimated project life of 20 years.

This project also provides for a vast future scope wherein many modifications and studies are possible using the same setup which is very useful as an academic pilot project. Implementation of solar tracking will allow for a further 3-5% increase in the energy harvested. Further, in-house design and fabrication of power electronic devices (Inverter and MPP tracker as well as BMS and charge controller) will aid in further reduction of cost and open up additional research areas. Also, the thermal behavior of both, the solar cells and Lithium-ion batteries can be studied parallel with pyrolysis production studies. With this data, an electrothermal model of the batteries could also be developed.

## VII. ACKNOWLEDGMENT

We would like to thank Prof. Abhishek P. S. Bhadauria who accepted us under his guidance for the project. He constantly motivated, guided and supported us on all endeavors throughout the duration of the project giving us valuable inputs at each stage. We are also thankful to Dr. Kashinath N. Patil for always being there whenever we had any technical difficulties and presenting us with different viewpoints and giving newer directions for development of the reactor. Lastly, we would like to thank K.J. Somaiya College of Engineering for providing a platform and facilities to further our engineering skills and knowledge.

## REFERENCES

[1] S. Bhuvaneshwari, Hiroshan Hettiarachchi, Jay N. Meegoda," Crop Residue Burning in India: Policy Challenges and Potential Solutions", PMCID: PMC6427124, 16(5): 832, 2019
[2] Suman, Santosh & Ahamad, Jameel,"Solar Energy Potential and Future Energy of India: An Overview", 2018..
[3] Mohammad I. Jahirul, Mohammad G. Rasul, 2012, "Biofuels Production through Biomass Pyrolysis —A Technological Review", Energies, 5, 4952-5001; doi:10.3390/en5124952, 2012
[4] Rajput, Saurabh, "SOLAR ENERGY- Fundamentals, Economic and Energy Analysis First Edition": ISBN: 978-93—81125-23—6, 2012.
[5] "Microtek 5KVA 48V MPPT inverter datasheet", Microtek, India, 2019.
[6] "Polycab Polycrystalline 72 cell module datasheet", Polycab, India, 2019.
[7] Arno HM Smets, Klaus Jäger, Olindo Isabella, René ACMM van Swaaij, Miro Zeman, "Solar energy: The physics and engineering of photovoltaic conversion, technologies and systems", 2015
[8] Mark Z. Jacobson, Vijaysinh Jadhav, "World estimates of PV optimal tilt angles and ratios of sunlight incident upon tilted and tracked PV panels relative to horizontal panels", 2018.
[9] Yu Miao 1 , Patrick Hynan , Annette von Jouanne and Alexandre Yokochi,"Current Li-Ion Battery Technologies in Electric Vehicles and Opportunities for Advancements", 2019.
[10] Chunjing Lin , Sichuan Xu , Zhao Li , Bin Li , Guofeng Chang , Jinling Liu, "Thermal analysis of large-capacity LiFePO4 power batteries for electric vehicles", 2015.
[11] "Electrical Power Engineering: Reference & Applications Handbook".
[12] Antonio Luque, Steven Hegedus, "Handbook of Photovoltaic Science and Engineering", 2011.

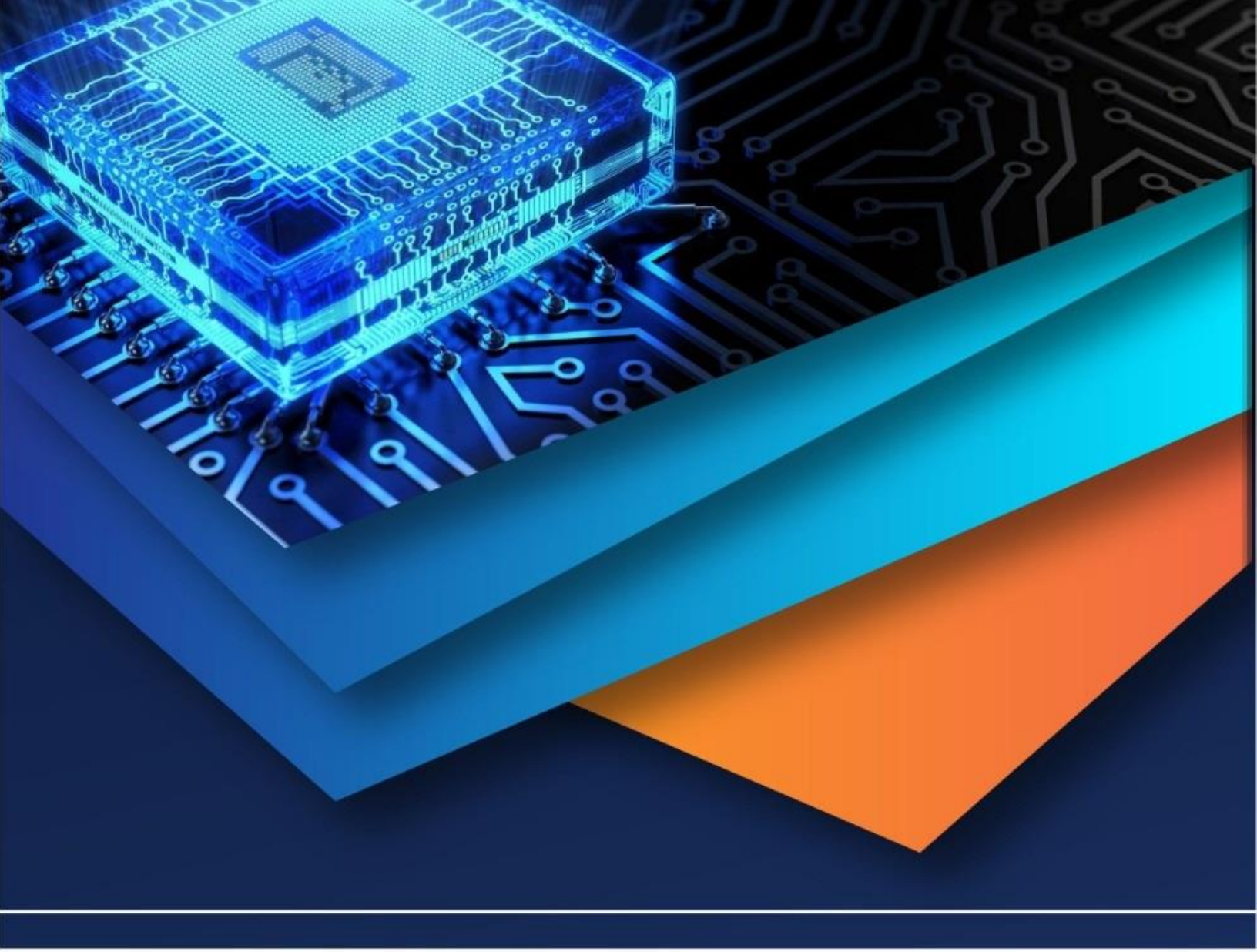

10.22214/IJRASET

45.98

IMPACT FACTOR: 7.129

IMPACT FACTOR: 7.429

# INTERNATIONAL JOURNAL FOR RESEARCH

IN APPLIED SCIENCE & ENGINEERING TECHNOLOGY